AIAA JOURNAL
Vol. 40, No. 2, February 2002

Dynamic Analysis of Flexible Beams Undergoing Overall Motion Employing Linear Strain Measures

Seok Seo* and Hong Hee Yoo†
Hanyang University, Seoul 133-791, Republic of Korea

A modeling method for the dynamic analysis of a flexible beam undergoing free overall motion is proposed. The overall motion is measured at a reference frame that is a rigid cross section of the beam. The elastic deformation is measured with respect to the reference frame and is expressed with deformation variables including a stretch variable. The use of a stretch variable leads to a simple linear strain measure and a corresponding quadratic strain energy expression. In spite of the simplicity, motion-induced stiffness variation effects, which are often critically important to the dynamic analysis of flexible structures undergoing overall motion, can be captured accurately by the modeling method. To demonstrate the accuracy of the modeling method, test problems are presented and solved. The present modeling method proves to be as accurate as a nonlinear finite element modeling method. Applicable ranges of the present modeling method are investigated through dimensional analysis and numerical study.

Nomenclature

A	=	reference frame that is the left-side cross section of the beam
$\boldsymbol{a}^P$	=	acceleration of the generic point P
$\hat{\boldsymbol{a}}_1, \hat{\boldsymbol{a}}_2, \hat{\boldsymbol{a}}_3$	=	orthogonal unit vectors fixed to the left-side cross section of the beam
B	=	reference frame that is the cross section where an external torque is applied
d_r	=	distance from point O to the point where an external force is applied
d_t	=	distance from point O to the center of the cross section where an external torque is applied
E	=	Young's modulus
F_i	=	generalized active forces
F_i^C	=	generalized active forces due to conservative forces
F_i^N	=	generalized active forces due to nonconservative forces
F_i^*	=	generalized inertia forces
I	=	area moment of inertia of the beam cross section
L	=	length of the beam
N	=	Newtonian reference frame
$\hat{\boldsymbol{n}}_1, \hat{\boldsymbol{n}}_2, \hat{\boldsymbol{n}}_3$	=	orthogonal unit vectors fixed to the Newtonian reference frame
p_i	=	generalized speeds
q_{1i}, q_{2i}	=	generalized coordinates related to elastic deformation
$\boldsymbol{R}$	=	external force vector
R_1, R_2	=	measuring numbers of $\boldsymbol{R}$ in the direction of $\hat{\boldsymbol{a}}_1$ and $\hat{\boldsymbol{a}}_2$
S	=	cross-sectional area of the beam
s	=	arc length stretch along the neutral axis
T	=	magnitude of $\boldsymbol{T}$
$\boldsymbol{T}$	=	external torque vector
$T_{\max}$	=	maximum value of T
$\bar{T}, \bar{R}_1, \bar{R}_2$	=	dimensionless forms of T, R_1, and R_2
$\bar{T}_{\max}, \bar{R}_{1,\max}, \bar{R}_{2,\max}$	=	maximum values of $\bar{T}$, $\bar{R}_1$, and $\bar{R}_2$
t_f	=	time duration while the external torque is active
t_s	=	time to reach the maximum value of torque
t^*	=	reference time
U	=	elastic strain energy of a beam
u_1, u_2	=	measuring numbers of deformation in the directions of $\hat{\boldsymbol{a}}_1$ and $\hat{\boldsymbol{a}}_2$
$\boldsymbol{v}^O$	=	velocity of point O
$\boldsymbol{v}^P$	=	velocity of the generic point P
$\boldsymbol{v}_i^P$	=	partial velocities of the generic point P
v_1, v_2	=	measuring numbers of the velocity of the generic point P in the directions of $\hat{\boldsymbol{a}}_1$ and $\hat{\boldsymbol{a}}_2$
x	=	distance from O to P_0
x^*, y^*	=	measuring numbers of the vector from O^* to O in the direction of $\hat{\boldsymbol{n}}_1$ and $\hat{\boldsymbol{n}}_2$
z_{ij}	=	dimensionless form of generalized coordinates related to elastic deformation
α	=	slenderness ratio
δ_r	=	applied force location ratio
δ_t	=	applied torque location ratio
ζ	=	dimensionless form of x
η	=	dimensionless time to reach the maximum value of external load
θ^*	=	angle between $\hat{\boldsymbol{n}}_1$ and $\hat{\boldsymbol{a}}_1$
μ	=	sum of μ_1 and μ_2
μ_1, μ_2	=	numbers of generalized coordinates for s and u_2
ρ	=	mass per unit length of the beam
σ, γ	=	dimensionless forms of x^* and y^*
τ	=	dimensionless time
ϕ_{1i}, ϕ_{2i}	=	spatial mode functions for s and u_2
$\boldsymbol{\omega}^A$	=	angular velocity of cross section A
$\boldsymbol{\omega}^B$	=	angular velocity of cross section B
$\boldsymbol{\omega}_i^B$	=	partial angular velocities of cross section B
ω_3	=	angular speed of cross section A
$'$	=	partial derivative of the symbol with respect to x
$''$	=	double differentiation of the symbol with respect to x
$\dot{}$	=	time derivative of the symbol

Received 22 August 2000; revision received 5 June 2001; accepted for publication 20 July 2001.

*Graduate Student, School of Mechanical Engineering, Sungdong-Gu Haengdang-Dong 17; ss386@chollian.net.

†Associate Professor, School of Mechanical Engineering, Sungdong-Gu Haengdang-Dong 17; hhyoo@email.hanyang.ac.kr. Member AIAA.

I. Introduction

STRUCTURES undergoing overall motion are often assumed as rigid bodies when their elastic deformation remains small during the overall motion. However, elastic deformation does not remain small in some cases. Flexible spacecraft structures, which may have large deformations during their operation, are such

examples. Furthermore, even small elastic deformation may have significant meaning for some cases, such as precision machines. In those cases, the elastic deformation as well as the overall motion should be analyzed accurately. The elastic deformation is generally coupled with the overall motion. Thus, an adequate dynamic modeling method, by which the elastic deformation as well as the overall motion can be analyzed simultaneously, is needed.

The most widely used modeling method by which the elastic deformation as well as the overall motion can be analyzed simultaneously is the classical linear modeling method (for instance, see Refs. 1–3). This modeling method employs Cartesian deformation variables and the linear Cauchy strain measures. It has several merits, such as simplicity of formulation, ease of implementation in finite element methods, and efficiency of computation, which results from the use of coordinate reduction techniques.[4,5] This modeling method, however, often provides erroneous results when structures undergo overall motion such as rotation. To resolve the problem of the classical linear modeling method, several nonlinear modeling methods[6–8] have been developed. With these nonlinear modeling methods, the accuracy problem could be resolved. However, serious computational inefficiency results from the nonlinearity, which disables the coordinate reduction techniques.

Recently a new linear modeling method for the dynamic analysis of a flexible beam undergoing overall motion was introduced.[9] This modeling method employs hybrid deformation variables (including a stretch variable) along with a special linear strain measure. With this modeling method, not only the accuracy problem of the classical linear modeling method but also the inefficiency problem of nonlinear modeling methods could be resolved. In Ref. 9, however, the overall motion was assumed to be prescribed so that only the effect of the overall motion on the elastic deformation could be analyzed. In other words, the effect of the elastic deformation on the overall motion has not been analyzed so far. Moreover, the effects of the external force and the external torque have not been incorporated into the modeling method. These effects were previously considered in other approaches but have never been considered in the approach employed in the present work. Furthermore, applicable ranges of the present modeling method (limiting external force and torque) have not been investigated in previous study.

The purpose of the present work is to propose a modeling method for a flexible beam undergoing free overall motion. Different from the previous work in Ref. 9, an external torque and an external force are considered, and the governing equations related to overall motion as well as elastic deformation are derived. The effect of the elastic deformation on the overall motion (as well as the effect of the overall motion on the elastic deformation) is investigated, and the accuracy of the modeling method is examined through comparing its numerical results to those of a nonlinear modeling method. In the present work, moreover, applicable ranges of the present modeling method are investigated by employing dimensionless equations of motion. The limiting external force and torque, which show the capability limit of the present modeling method, are found. Therefore, the extension of the formulation and the investigation of the capability limit of the previous work (in Ref. 9) constitute the main contribution of the present work.

II. Equations of Motion

In this section, the procedure of deriving equations of motion of a beam undergoing free overall motion is presented. The method of Kane and Levinson[10] is employed to derive the equations of motion. To explain the procedure of deriving equations of motion in a simple and easy way (while exhibiting the key ingredients of the proposed modeling method), the following assumptions are made. The overall motion and the elastic deformation are constrained to occur in a plane. The beam has slender shape so that the shear and the rotary inertia effects are ignored. Thus, Euler–Bernoulli beam theory is employed. The beam has homogeneous and isotropic material properties. Any of these assumptions can be removed, if necessary, to obtain more general equations of motion.

Figure 1 shows the configuration of a deformed beam undergoing free overall motion in a plane. Any cross section of the beam can be regarded as a reference frame because it is assumed to rotate rigidly

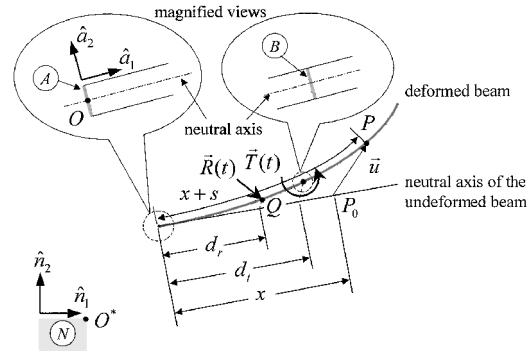

Fig. 1 Configuration of a deformed beam undergoing free overall motion.

in Euler–Bernoulli beam theory. Two reference frames are chosen from the cross sections of the beam. The first one is the left-side cross section of the beam, A, to which mutually orthogonal unit vectors $\hat{\boldsymbol{a}}_i$ are fixed. Point O is located at the neutral axis of cross section A. Elastic deformation is measured with respect to reference frame A. The second one is cross section B, where an external torque $\boldsymbol{T}$ is applied. The Newtonian reference frame N, which is fixed in space, is also shown in Fig. 1. Point O^* and mutually orthogonal unit vectors $\hat{\boldsymbol{n}}_i$ are fixed to the Newtonian reference frame. An external force $\boldsymbol{R}$ is applied to an arbitrary point Q. The generic point P_0 moves to P after elastic deformation occurs. The elastic deformation vector $\boldsymbol{u}$ is expressed as follows:

$$\boldsymbol{u} = u_1\hat{\boldsymbol{a}}_1 + u_2\hat{\boldsymbol{a}}_2 \tag{1}$$

The velocity of point O and the angular velocity of cross section A are given as follows:

$$\boldsymbol{v}^O = \dot{x}^*\hat{\boldsymbol{n}}_1 + \dot{y}^*\hat{\boldsymbol{n}}_2 = v_1\hat{\boldsymbol{a}}_1 + v_2\hat{\boldsymbol{a}}_2 \tag{2}$$

$$\boldsymbol{\omega}^A = \dot{\theta}^*\hat{\boldsymbol{n}}_3 = \omega_3\hat{\boldsymbol{a}}_3 \tag{3}$$

By the use of Eqs. (2) and (3), the velocity and the acceleration of the generic point P can be obtained as follows:

$$\boldsymbol{v}^P = (v_1 + \dot{u}_1 - \omega_3 u_2)\,\hat{\boldsymbol{a}}_1 + \{v_2 + \dot{u}_2 + \omega_3(x+u_1)\}\,\hat{\boldsymbol{a}}_2 \tag{4}$$

$$\boldsymbol{a}^P = \left\{\dot{v}_1 + \ddot{u}_1 - \dot{\omega}_3 u_2 - 2\omega_3\dot{u}_2 - \omega_3 v_2 - \omega_3^2(x+u_1)\right\}\hat{\boldsymbol{a}}_1 + \left\{\dot{v}_2 + \ddot{u}_2 + \dot{\omega}_3(x+u_1) + 2\omega_3\dot{u}_1 + \omega_3 v_1 - \omega_3^2 u_2\right\}\hat{\boldsymbol{a}}_2 \tag{5}$$

Because the shear effect is assumed to be negligible, the angular velocity of cross section B can be obtained as follows:

$$\boldsymbol{\omega}^B = \left(\omega_3 + \left.\frac{\partial \dot{u}_2}{\partial x}\right|_{x=d_t}\right)\hat{\boldsymbol{a}}_3 \tag{6}$$

In the classical linear modeling method, u_1 and u_2 are approximated to derive the ordinary differential equations of motion. In this modeling method, however, the arc length stretch along the neutral axis of the beam, s, is approximated along with the lateral displacement u_2 as follows:

$$s = \sum_{i=1}^{\mu_1} \phi_{1i}(x)q_{1i}(t) \tag{7}$$

$$u_2 = \sum_{i=1}^{\mu_2} \phi_{2i}(x)q_{2i}(t) \tag{8}$$

where $\phi_{1i}(x)$ and $\phi_{2i}(x)$ are spatial mode functions for s and u_2. Any compact set of mode functions that satisfies the boundary conditions of the beam can be used. Because s instead of u_1 is approximated in this modeling method, u_1 and $\dot{u}_1$ need be expressed in terms of s, u_2, $\dot{s}$, and $\dot{u}_2$. For this purpose, the following geometric relation between s and the Cartesian variables is employed:

$$x+s=\int_0^x\left[\left(1+\frac{\partial u_1}{\partial\xi}\right)^2+\left(\frac{\partial u_2}{\partial\xi}\right)^2\right]^{\frac{1}{2}}\mathrm{d}\xi \tag{9}$$

Using the binomial expansion theorem, Eq. (9) can be approximated (without affecting the final equations of motion, which are linear in terms of q_{1i} and q_{2i}) as follows:

$$s=u_1+\frac{1}{2}\int_0^x\left(\frac{\partial u_2}{\partial\xi}\right)^2\mathrm{d}\xi \tag{10}$$

Differentiation of the preceding equation with respect to time results in the following equation:

$$\dot{s}=\dot{u}_1+\int_0^x\left(\frac{\partial u_2}{\partial\xi}\right)\left(\frac{\partial\dot{u}_2}{\partial\xi}\right)\mathrm{d}\xi \tag{11}$$

Using Eqs. (4), (6–8), (10), and (11), the partial velocities of point P and the partial angular velocities of the cross section B can be obtained from the following equation:

$$\boldsymbol{v}_i^P=\frac{\partial\boldsymbol{v}^P}{\partial p_i}\qquad(i=1,2,\ldots,\mu+3) \tag{12}$$

$$\boldsymbol{\omega}_i^B=\frac{\partial\boldsymbol{\omega}^B}{\partial p_i}\qquad(i=1,2,\ldots,\mu+3) \tag{13}$$

where p_i are given as follows:

$$p_i=\dot{q}_{1i}\qquad(i=1,2,\ldots,\mu_1) \tag{14}$$

$$p_{i+\mu_1}=\dot{q}_{2i}\qquad(i=1,2,\ldots,\mu_2) \tag{15}$$

$$p_{\mu+1}=v_1 \tag{16}$$

$$p_{\mu+2}=v_2 \tag{17}$$

$$p_{\mu+3}=\omega_3 \tag{18}$$

The partial velocities of point Q can be obtained from those of point P by substituting a specific value for x, that is, $x=d_r$.

Because the rotary inertia effect is ignored, the generalized inertia forces of the beam are obtained from the following equation:

$$F_i^*=-\int_0^L\rho\boldsymbol{a}^P\cdot\boldsymbol{v}_i^P\,\mathrm{d}x\qquad(i=1,2,\ldots,\mu+3) \tag{19}$$

The generalized active forces of the beam can be obtained from the following equation:

$$F_i=F_i^C+F_i^N\qquad(i=1,2,\ldots,\mu+3) \tag{20}$$

F_i^C and F_i^N can be obtained from the following equations:

$$F_i^C=-\frac{\partial U}{\partial q_{1i}}\qquad(i=1,2,\ldots,\mu_1) \tag{21}$$

$$F_{i+\mu_1}^C=-\frac{\partial U}{\partial q_{2i}}\qquad(i=1,2,\ldots,\mu_2) \tag{22}$$

$$F_{\mu+i}^C=0\qquad(i=1,2,3) \tag{23}$$

$$F_i^N=\boldsymbol{T}\cdot\boldsymbol{\omega}_i^B+\boldsymbol{R}\cdot\boldsymbol{v}_i^Q\qquad(i=1,2,\ldots,\mu+3) \tag{24}$$

U shown in Eqs. (21) and (22) represents the elastic strain energy of a beam and is given as follows:

$$U=\frac{1}{2}\int_0^L ES\left(\frac{\partial s}{\partial x}\right)^2\mathrm{d}x+\frac{1}{2}\int_0^L EI\left(\frac{\partial^2u_2}{\partial x^2}\right)^2\mathrm{d}x \tag{25}$$

The generalized inertia forces and the generalized active forces constitute the equations of motion as follows:

$$F_i^*+F_i=0\qquad(i=1,2,\ldots,\mu+3) \tag{26}$$

When the terms that are nonlinear in terms of q_{1i} and q_{2i} are truncated, the resulting equations of motion can be obtained as follows:

$$\begin{aligned}&\sum_{j=1}^{\mu_1}m_{ij}^{11}\ddot{q}_{1j}-\dot{\omega}_3\sum_{j=1}^{\mu_2}m_{ij}^{12}q_{2j}-2\omega_3\sum_{j=1}^{\mu_2}m_{ij}^{12}\dot{q}_{2j}\\&\quad-\omega_3^2\sum_{j=1}^{\mu_1}m_{ij}^{11}q_{1j}+\sum_{j=1}^{\mu_1}k_{ij}^Sq_{1j}=-(\dot{v}_1-\omega_3v_2)P_{1i}\\&\quad+\omega_3^2Q_{1i}+R_1\phi_{1i}(d_r)\qquad(i=1,2,\ldots,\mu_1)\end{aligned} \tag{27}$$

$$\begin{aligned}&\sum_{j=1}^{\mu_2}m_{ij}^{22}\ddot{q}_{2j}-\omega_3^2\sum_{j=1}^{\mu_2}m_{ij}^{22}q_{2j}+\dot{\omega}_3\sum_{j=1}^{\mu_1}m_{ij}^{21}q_{1j}+2\omega_3\sum_{j=1}^{\mu_1}m_{ij}^{21}\dot{q}_{1j}\\&\quad-(\dot{v}_1-\omega_3v_2)\sum_{j=1}^{\mu_2}k_{ij}^{GA}q_{2j}+\omega_3^2\sum_{j=1}^{\mu_2}k_{ij}^{GB}q_{2j}+\sum_{j=1}^{\mu_2}k_{ij}^Bq_{2j}\\&\quad=-(\dot{v}_2+\omega_3v_1)P_{2i}-\dot{\omega}_3Q_{2i}-R_1\sum_{j=1}^{\mu_2}k_{ij}^Rq_{2j}\\&\quad+R_2\phi_{2i}(d_r)+T(t)\phi_{2i,x}(d_t)\qquad(i=1,2,\ldots,\mu_2)\end{aligned} \tag{28}$$

$$\begin{aligned}&(\dot{v}_1-\omega_3v_2)\rho L-\dot{\omega}_3\sum_{j=1}^{\mu_2}P_{2j}q_{2j}+\sum_{j=1}^{\mu_1}P_{1j}\ddot{q}_{1j}\\&\quad-2\omega_3\sum_{j=1}^{\mu_2}P_{2j}\dot{q}_{2j}-\frac{1}{2}\rho L^2\omega_3^2-\omega_3^2\sum_{j=1}^{\mu_1}P_{1j}q_{1j}=R_1\end{aligned} \tag{29}$$

$$\begin{aligned}&(\dot{v}_2+\omega_3v_1)\rho L+\sum_{j=1}^{\mu_2}P_{2j}\ddot{q}_{2j}+\frac{1}{2}\rho L^2\dot{\omega}_3+\dot{\omega}_3\sum_{j=1}^{\mu_1}P_{1j}q_{1j}\\&\quad+2\omega_3\sum_{j=1}^{\mu_1}P_{1j}\dot{q}_{1j}-\omega_3^2\sum_{j=1}^{\mu_2}P_{2j}q_{2j}=R_2\end{aligned} \tag{30}$$

$$\begin{aligned}&\frac{1}{3}\rho L^3\dot{\omega}_3+2\dot{\omega}_3\sum_{j=1}^{\mu_1}Q_{1j}q_{1j}-(\dot{v}_1-\omega_3v_2)\sum_{j=1}^{\mu_2}P_{2j}q_{2j}\\&\quad+\frac{1}{2}(\dot{v}_2+\omega_3v_1)\rho L^2+(\dot{v}_2+\omega_3v_1)\sum_{j=1}^{\mu_1}P_{1j}q_{1j}\\&\quad+\sum_{j=1}^{\mu_2}Q_{2j}\ddot{q}_{2j}+2\omega_3\sum_{j=1}^{\mu_1}Q_{1j}\dot{q}_{1j}=-R_1\sum_{j=1}^{\mu_2}\phi_{2j}(d_r)q_{2j}\\&\quad+R_2\left(d_r+\sum_{j=1}^{\mu_1}\phi_{1j}(d_r)q_{1j}\right)+T\end{aligned} \tag{31}$$

where

$$k_{ij}^S=\int_0^L ES\phi_{1i,x}\phi_{1j,x}\,\mathrm{d}x \tag{32}$$

$$k_{ij}^B=\int_0^L EI\phi_{2i,xx}\phi_{2j,xx}\,\mathrm{d}x \tag{33}$$

$$P_{\alpha i}=\int_0^L\rho\phi_{\alpha i}\,\mathrm{d}x \tag{34}$$

$$Q_{\alpha i}=\int_0^L\rho x\phi_{\alpha i}\,\mathrm{d}x \tag{35}$$

$$m_{ij}^{\alpha\beta}=\int_0^L\rho\phi_{\alpha i}\phi_{\beta j}\,\mathrm{d}x \tag{36}$$

$$k_{ij}^{GA} = \int_0^L \rho(L-x)\phi_{2i,x}\phi_{2j,x}\,\mathrm{d}x \tag{37}$$

$$k_{ij}^{GB} = \frac{1}{2}\int_0^L \rho(L^2-x^2)\phi_{2i,x}\phi_{2j,x}\,\mathrm{d}x \tag{38}$$

$$k_{ij}^{R} = \int_0^{d_r} \phi_{2i,x}\phi_{2j,x}\,\mathrm{d}x \tag{39}$$

If the classical linear modeling method were employed to derive the equations of motion, the terms involving k_{ij}^{GA} and k_{ij}^{GB} in Eq. (28) would not appear. These terms are often called the motion-induced stiffness variation terms. Without these terms, the classical linear modeling method often provides erroneous results. As shown in Eq. (28), the stiffness variations become significant when $(\dot{v}_1 - \omega_3 v_2)$ or ω_3^2 are significant. It can be interpreted that the stiffness variation terms become significant when the large overall motion induces a stretching (or compressing) effect to the beam.

In the following section, the applicable ranges of the present modeling method will be discussed. For this purpose, the dimensionless equations of motion need to be derived. To derive dimensionless equations of motion, the dimensionless variables are defined as follows:

$$\tau = t/t^* \tag{40}$$

$$\zeta = x/L \tag{41}$$

$$z_{ij} = q_{ij}/L \tag{42}$$

$$\sigma = x^*/L \tag{43}$$

$$\gamma = y^*/L \tag{44}$$

$$\omega = t^*\omega_3 \tag{45}$$

where

$$t^* = \sqrt{\rho L^4/EI} \tag{46}$$

When these dimensionless variables are used, the dimensionless equations of motion can be obtained as follows:

$$\sum_{j=1}^{\mu_1} \bar{M}_{ij}^{11}\ddot{z}_{1j} - \dot{\omega}\sum_{j=1}^{\mu_2} \bar{M}_{ij}^{12} z_{2j} - 2\omega\sum_{j=1}^{\mu_2} \bar{M}_{ij}^{12}\dot{z}_{2j} - \omega^2\sum_{j=1}^{\mu_1} \bar{M}_{ij}^{11} z_{1j} + \alpha^2\sum_{j=1}^{\mu_1} \bar{K}_{ij}^{S} z_{1j} = -(\dot{\beta}_1 - \omega\beta_2)\bar{P}_{1i} + \omega^2\bar{Q}_{1i} + \bar{R}_1\psi_{1i}(\delta_r) \qquad (i = 1, 2, \ldots, \mu_1) \tag{47}$$

$$\sum_{j=1}^{\mu_2} \bar{M}_{ij}^{22}\ddot{z}_{2j} - \omega^2\sum_{j=1}^{\mu_2} \bar{M}_{ij}^{22} z_{2j} + \dot{\omega}\sum_{j=1}^{\mu_1} \bar{M}_{ij}^{21} z_{1j} + 2\omega\sum_{j=1}^{\mu_1} \bar{M}_{ij}^{21}\dot{z}_{1j} - (\dot{\beta}_1 - \omega\beta_2)\sum_{j=1}^{\mu_2} \bar{K}_{ij}^{GA} z_{2j} + \omega^2\sum_{j=1}^{\mu_2} \bar{K}_{ij}^{GB} z_{2j} + \sum_{j=1}^{\mu_2} \bar{K}_{ij}^{B} z_{2j} = -(\dot{\beta}_2 + \omega\beta_1)\bar{P}_{2i} - \dot{\omega}\bar{Q}_{2i} - \bar{R}_1\sum_{j=1}^{\mu_2} \bar{K}_{ij}^{R} z_{2j} + \bar{R}_2\psi_{2i}(\delta_r) + \bar{T}\psi_{2i,\zeta}(\delta_t) \qquad (i = 1, 2, \ldots, \mu_2) \tag{48}$$

$$(\dot{\beta}_1 - \omega\beta_2) + \sum_{j=1}^{\mu_1} \bar{P}_{1j}\ddot{z}_{1j} - \dot{\omega}\sum_{j=1}^{\mu_2} \bar{P}_{2j} z_{2j} - 2\omega\sum_{j=1}^{\mu_2} \bar{P}_{2j}\dot{z}_{2j} - \frac{1}{2}\omega^2 - \omega^2\sum_{j=1}^{\mu_1} \bar{P}_{1j} z_{1j} = \bar{R}_1 \tag{49}$$

$$(\dot{\beta}_2 + \omega\beta_1) + \sum_{j=1}^{\mu_2} \bar{P}_{2j}\ddot{z}_{2j} + \frac{1}{2}\dot{\omega} + \dot{\omega}\sum_{j=1}^{\mu_1} \bar{P}_{1j} z_{1j} + 2\omega\sum_{j=1}^{\mu_1} \bar{P}_{1j}\dot{z}_{1j} - \omega^2\sum_{j=1}^{\mu_2} \bar{P}_{2j} z_{2j} = \bar{R}_2 \tag{50}$$

$$-(\dot{\beta}_1 - \omega\beta_2)\sum_{j=1}^{\mu_2} \bar{P}_{2j} z_{2j} + \frac{1}{2}(\dot{\beta}_2 + \omega\beta_1) + (\dot{\beta}_2 + \omega\beta_1)\sum_{j=1}^{\mu_1} \bar{P}_{1j} z_{1j} + \frac{1}{3}\dot{\omega} + 2\dot{\omega}\sum_{j=1}^{\mu_1} \bar{Q}_{1j} z_{1j} + \sum_{j=1}^{\mu_2} \bar{Q}_{2j}\ddot{z}_{2j} + 2\omega\sum_{j=1}^{\mu_1} \bar{Q}_{1j}\dot{z}_{1j} = -\bar{R}_1\sum_{j=1}^{\mu_2} \psi_{2j}(\delta_r) z_{2j} + \bar{R}_2\left(\delta_r + \sum_{j=1}^{\mu_1} \psi_{1j}(\delta_r) z_{1j}\right) + \bar{T} \tag{51}$$

where

$$\delta_r = \frac{d_r}{L} \tag{52}$$

$$\delta_t = \frac{d_t}{L} \tag{53}$$

$$\alpha = \sqrt{\frac{SL^2}{I}} \tag{54}$$

$$\bar{R}_1 = \frac{R_1 L^2}{EI} \tag{55}$$

$$\bar{R}_2 = \frac{R_2 L^2}{EI} \tag{56}$$

$$\bar{T} = \frac{TL}{EI} \tag{57}$$

$$\bar{K}_{ij}^{S} = \int_0^1 \psi_{1i,\zeta}\psi_{1j,\zeta}\,\mathrm{d}\zeta \tag{58}$$

$$\bar{K}_{ij}^{B} = \int_0^1 \psi_{2i,\zeta\zeta}\psi_{2j,\zeta\zeta}\,\mathrm{d}\zeta \tag{59}$$

$$\bar{P}_{\alpha i} = \int_0^1 \psi_{\alpha i}\,\mathrm{d}\zeta \tag{60}$$

$$\bar{Q}_{\alpha i} = \int_0^1 \zeta\,\psi_{\alpha i}\,\mathrm{d}\zeta \tag{61}$$

$$\bar{M}_{ij}^{\alpha\beta} = \int_0^1 \psi_{\alpha i}\psi_{\beta i}\,\mathrm{d}\zeta \tag{62}$$

$$\bar{K}_{ij}^{GA} = \int_0^1 (1-\zeta)\psi_{2i,\zeta}\psi_{2j,\zeta}\,\mathrm{d}\zeta \tag{63}$$

$$\bar{K}_{ij}^{GB} = \int_0^1 (1-\zeta^2)\psi_{2i,\zeta}\psi_{2j,\zeta}\,\mathrm{d}\zeta \tag{64}$$

$$\bar{K}_{ij}^{R} = \int_0^{\delta_r} \psi_{2i,\zeta}\psi_{2j,\zeta}\,\mathrm{d}\zeta \tag{65}$$

$$\beta_1 = \cos\theta^*\dot{\sigma} + \sin\theta^*\dot{\gamma} \tag{66}$$

$$\beta_2 = -\sin\theta^*\dot{\sigma} + \cos\theta^*\dot{\gamma} \tag{67}$$

III. Numerical Study

In this section, numerical examples are presented and solved to exhibit the integrity of the proposed modeling method. To solve the

equations of motion, two stretching and three bending mode functions, which are proven to be sufficient for the solution convergence through numerical study, are employed. The eigenfunctions of a cantilever beam (obtained from the longitudinal and the bending vibration analysis) are used as the mode functions. For numerical integration, a fourth-order variable step Runge–Kutta method is used. A nonlinear finite element commercial code[11,12] is employed to produce numerical results to which those of the present modeling method are compared.

For the first problem, the beam undertakes only an external torque, which is applied to one of the three points shown in Fig. 2a. The data used for the problem are given in Table 1. The function of the torque is given as follows:

$$\text{if} \quad 0 \le t < t_f, \qquad T(t) = \tfrac{1}{2} T_{\max}[1 - \cos(2\pi t / t_f)]$$

$$\text{elsewhere} \qquad T(t) = 0 \tag{68}$$

This function varies smoothly so that it can avoid any numerical trouble due to discontinuities during the integration.

Figure 3 shows the bending deflections of the right endpoint of the beam, which are measured with respect to the left endpoint by using the coordinate system attached to the left-end cross section of the beam. The external torque is applied to the right endpoint (case 1 in Fig. 2a). The solid line represents the result obtained by the present modeling method, and the dotted line represents that obtained by the classical linear modeling method. It is shown that the classical linear modeling method provides a diverging result whereas the present modeling method provides a well converging result. As already discussed, the equations of motion obtained by the classical linear modeling method do not include the motion-induced stiffness variation terms [shown in Eq. (28)], and the absence of those terms results in the qualitatively different response as shown in Fig. 3.

Figures 4 and 5 show the bending deflections of the right endpoint of the beam, which are measured with respect to the left endpoint by using the coordinate system attached to the left-end cross section of the beam. Two cases of simulations are made (cases 2 and 3 in Fig. 2a). The external torque is applied to the left endpoint in the first case and the middle point in the second case. Solid lines represent the results obtained by the present modeling method, and dotted lines represent the results obtained by a nonlinear finite element commercial code. The results obtained by the two methods are shown to be in good agreement overall. Figures 4 and 5, however, show that the commercial code provides somewhat disturbing responses, whereas the present modeling method provides smooth plausible responses. Artificial damping is often used to remedy the problem of disturbing responses obtained with the nonlinear finite element commercial code. Determining the amount of artificial damping is sometimes a nuisance. Figure 6 shows the trajectories of the left endpoint of the beam for the first case of simulation that are obtained by using the

Table 1 Simulation data for numerical examples

Notation	First problem	Second problem
Mass per unit length ρ, kg/m	1.2	1.0
Young's modulus E, GPa	70.0	1.0
Length L, m	10	10
Cross-sectional area S, m^2	4.0E–4	1.0E–5
Area moment of inertia I, m^4	2.0E–7	5.0E–7
Maximum value of torque $T_{\max}$, N · m	150	40
Time to reach the maximum value of torque t_s, s	——	2
Time duration while the external torque is active t_f, s	10	5

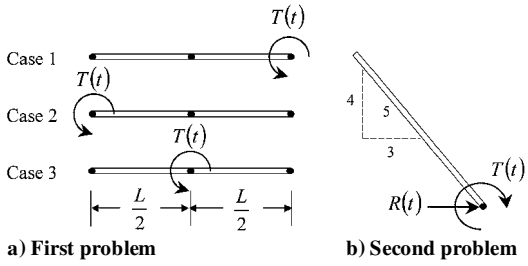

Fig. 2 Description of external load for the first and the second problems.

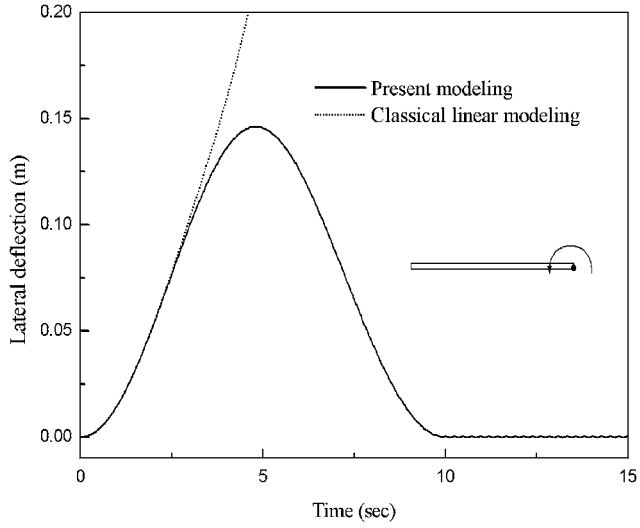

Fig. 3 Comparison of lateral deflections obtained by the present and classical linear modeling methods.

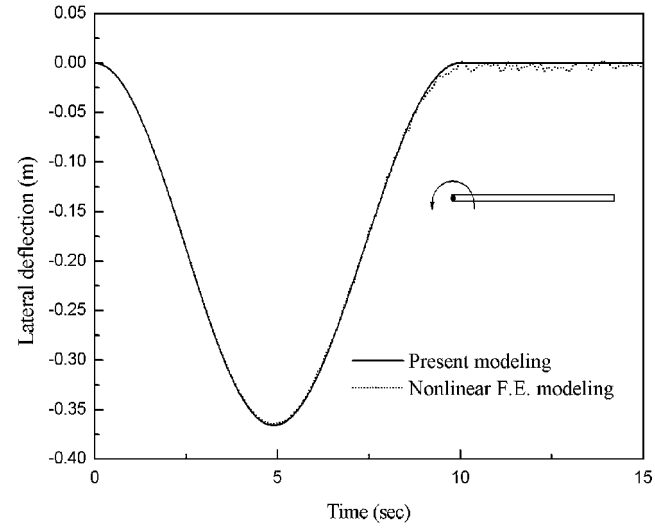

Fig. 4 Lateral deflection of the beam (torque applied to left endpoint).

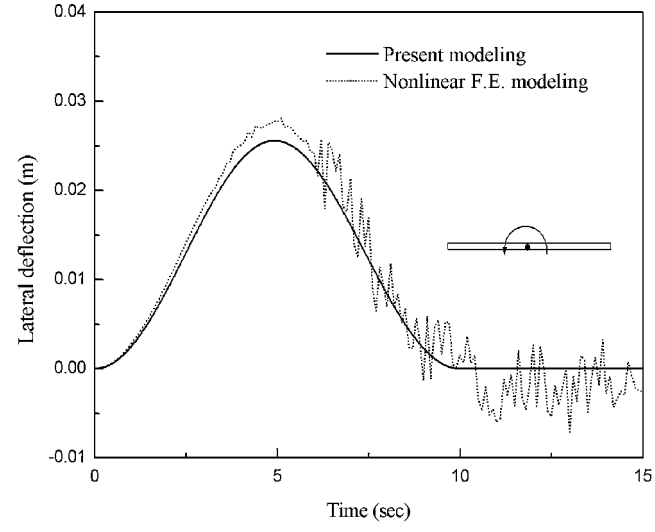

Fig. 5 Lateral deflection of the beam (torque applied to middle point).

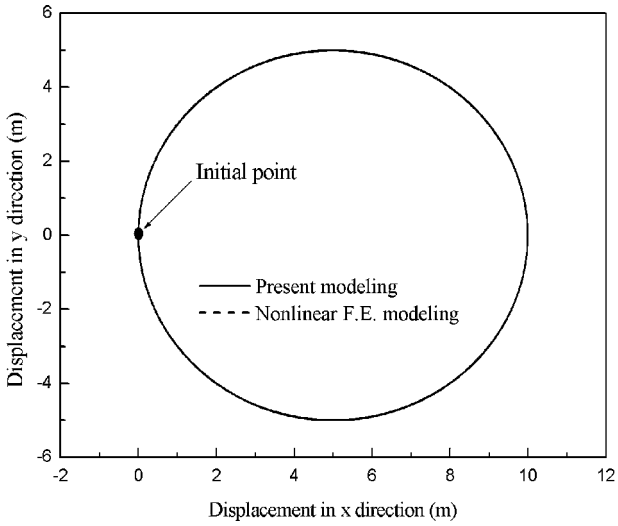

Fig. 6 Trajectory of the left endpoint of beam for the first problem.

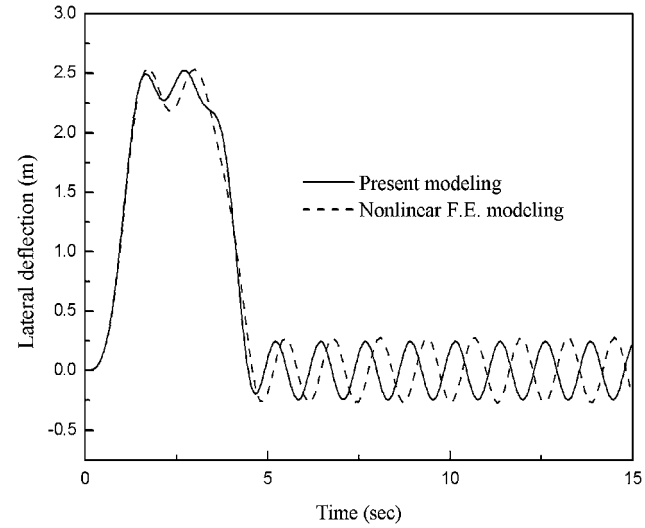

Fig. 7 Lateral deflection of the beam for the second problem.

present modeling method and the nonlinear finite element modeling method. It is shown that the two results are almost identical.

For the second problem, an external force, as well as an external torque, is applied to the beam. The external torque is given as follows:

$$\text{if} \quad 0 \le t < t_s, \qquad T(t) = T_{\max}\left(\frac{t}{t_s} - \frac{1}{2\pi}\sin\frac{2\pi t}{t_s}\right)$$

$$\text{if} \quad t_s \le t < t_f - t_s, \qquad T(t) = T_{\max}$$

$$\text{if} \quad t_f - t_s \le t < t_f, \qquad T(t) = T_{\max}\left[\frac{t_f - t}{t_s} - \frac{1}{2\pi}\sin\frac{2\pi(t_f - t)}{t_s}\right]$$

$$\text{elsewhere} \qquad T(t) = 0 \tag{69}$$

The external force $\boldsymbol{R}$ is given as follows:

$$\boldsymbol{R} = R(t)\hat{\boldsymbol{n}}_1 \tag{70}$$

where

$$R(t) = T(t)/10 \tag{71}$$

The data used for the second problem are also given in Table 1. As shown in Table 1, the beam is very flexible (see Young's modulus). The external torque and the external force are applied to the left endpoint of the beam, as shown in Fig 2b.

Figure 7 shows the bending deflections of the right endpoint of the beam, which are measured with respect to the left endpoint by using the coordinate system attached to the left-end cross section of the beam. The solid line represents the result obtained by the present modeling method, and the dotted line represents that obtained by the nonlinear finite element modeling method. The the two results appear to be in good agreement in the transient region, although they show some phase difference in the steady-state region. The difference results from the artificial numerical damping added to the nonlinear finite element modeling. Without the artificial numerical damping, numerical integration failures are often encountered during the integration. Because of the damping effect, the natural frequency of the steady-state response obtained by the nonlinear finite element modeling method is shown to be lowered slightly.

Figure 8 shows the trajectory of the left endpoint of the beam during the simulation. For the same reason, that is, artificial numerical damping, a small amount of difference between the two results exists. Figure 9 shows 20 configurations of the beam. The bold lines are the configurations of the beam at the moment of 3 and 13 s after the simulation starts. The other 18 configurations are drawn at 18 moments at a 0.5-s interval. Figure 9 shows the overall motion including the elastic deformation. To investigate the effect of the elastic deformation on the overall motion of the beam, the results

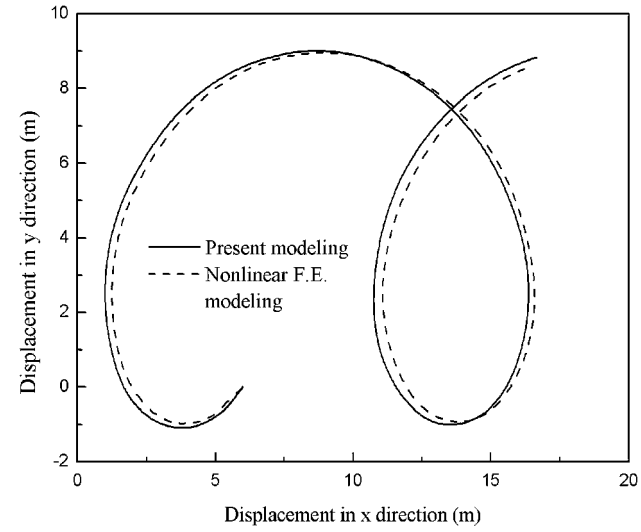

Fig. 8 Trajectory of the left endpoint of beam for the second problem.

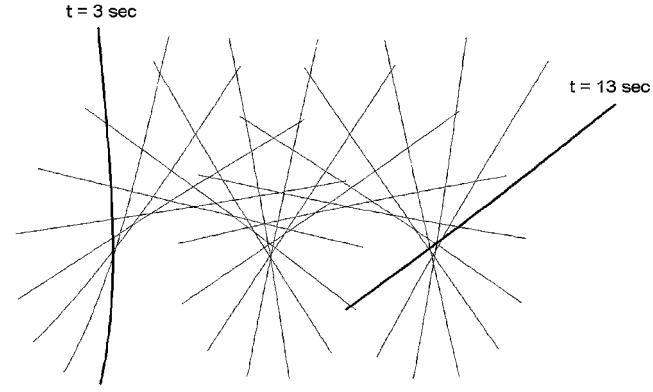

Fig. 9 Flight configurations of the beam for the second problem.

of overall motion with different bending stiffnesses are compared. Figure 10 shows the difference between rigid-body rotating angles with $EI = 500$ (which is given in Table 1) and $EI = 5000$. This shows that the overall motion is clearly influenced by the flexibility of the beam, which is related to the elastic deformation.

The limitations of the present modeling method were discovered during the numerical study. The system mass matrix, which consists of the coefficients of the highest-order terms in Eqs. (27–31), becomes singular when the maximum external load increases or the time t_s to reach the maximum torque decreases. In other words,

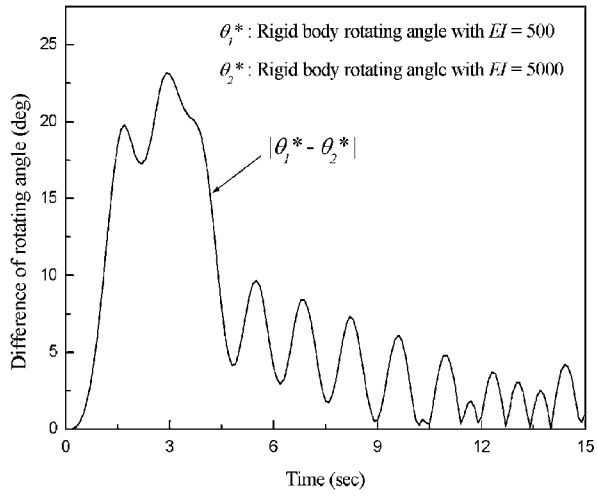

Fig. 10 Difference between two rigid-body rotating angles.

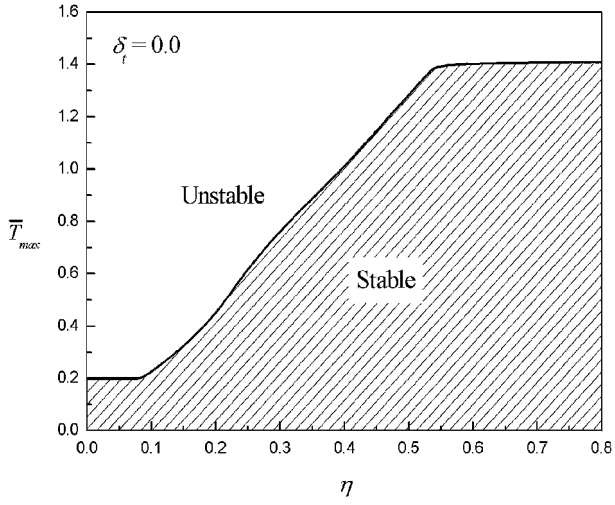

Fig. 11 Stability diagram of time integration related to external torque $\bar{T}$.

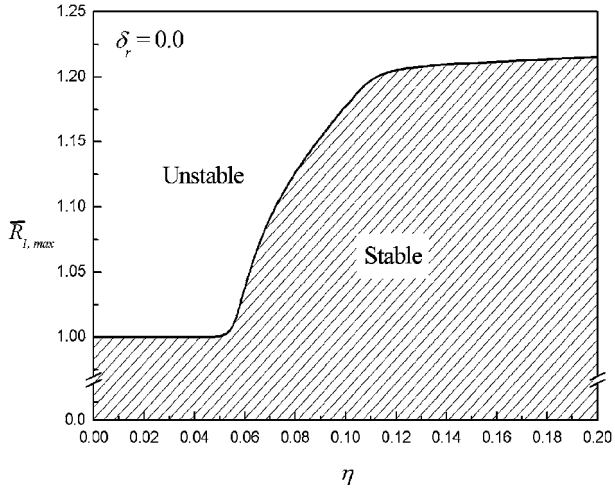

Fig. 12 Stability diagram of time integration related to longitudinal external force $\bar{R}_1$.

abrupt large external loads generally result in numerical integration failures. To identify the parameters and their ranges that cause the trouble, dimensionless equations of motion (which are derived in the preceding section) are employed. It is found that $\bar{T}_{\max}$, $\bar{R}_{1,\max}$, $\bar{R}_{2,\max}$, and η are related to the trouble, where η is given by

$$\eta = t_s / t^* \tag{72}$$

Figures 11–13 are stability diagrams in which parametric regions for successful and unsuccessful time integrations are shown. Typical

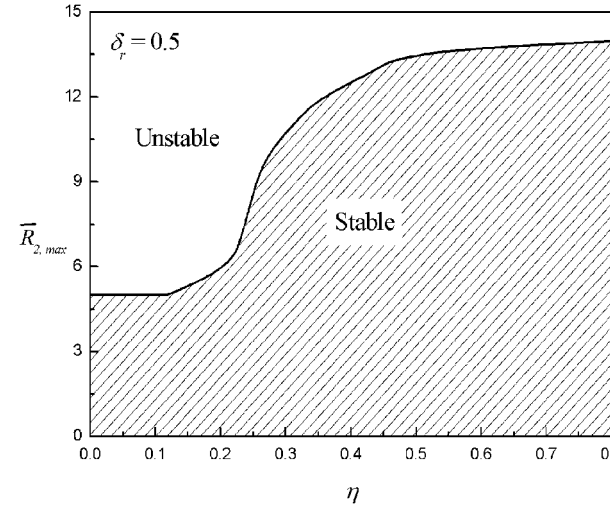

Fig. 13 Stability diagram of time integration related to lateral external force $\bar{R}_2$.

locations of external load (torque or force) are chosen and described in Figs. 11–13. In Fig. 11, the transition curve that divides the two regions rises monotonically as $\bar{T}_{\max}$ increases. If $\bar{T}_{\max}$ increases, η should be increased to avoid the integration failure. Figures 12 and 13 show that similar phenomena occur with $\bar{R}_{1,\max}$ and $\bar{R}_{2,\max}$. It can be also found that successful integrations can be always achieved when external loads are smaller than certain values. On the contrary, integration failures always occur when external loads are larger than certain values.

IV. Conclusions

In the present work, a modeling method is proposed for the dynamic analysis of a flexible beam undergoing free overall motion. The modeling method employs hybrid deformation variables including a stretch variable and corresponding linear strain measures. Even though linear strain measures are employed, the stiffness variation effects induced by overall motion, which are often critically important to the dynamic analysis of flexible structures, can be captured accurately by the modeling method. To demonstrate the accuracy of the modeling method, numerical examples are solved, and the results of the present modeling method are compared to those of a nonlinear finite element modeling method. The numerical results obtained by the present modeling method are found to be overall in good agreement with those obtained by a nonlinear finite element modeling method. The present modeling method, however, has limitations in applicable ranges. Abrupt or large external loads often cause integration failures. Dimensionless parameters related to external loads are identified, and their parametric regions for successful (or unsuccessful) time integration are obtained.

Acknowledgment

This research was supported by Center of Innovative Design Optimization Technology, Korea Science and Engineering Foundation.

References

[1]Frisch, H., "A Vector-Dyadic Development of the Equations of Motion for N-Coupled Flexible Bodies and Point Masses," NASA TN D-8047, 1975.

[2]Ho, J., "Direct Path Method for Flexible Multibody Spacecraft Dynamics," *Journal of Spacecraft and Rockets*, Vol. 14, No. 2, 1977, pp. 102–110.

[3]Bodley, C., Devers, A., Park, A., and Frisch, H., "A Digital Computer Program for the Dynamic Interaction Simulation of Controls and Structure," Vols. 1 and 2, NASA TP-1219, May 1978.

[4]Hurty, W., Collins, J., and Hart, G., "Dynamic Analysis of Large Structures by Modal Synthesis Techniques," *Computers and Structures*, Vol. 1, Aug. 1971, pp. 535–563.

[5]Hale, A. L., and Meirovitch, L., "A General Substructure Synthesis Method for the Dynamic Simulation of Complex Structures," *Journal of Sound and Vibration*, Vol. 69, No. 2, 1980, pp. 309–326.

[6]Belytschko, T., and Hsieh, B., "Non-Linear Transient Finite Element Analysis with Convected Coordinates," *International Journal for Numerical Methods in Engineering*, Vol. 7, No. 3, 1973, pp. 255–271.

[7]Simo, J. C., and Vu-Quoc, L., "On the Dynamics of Flexible Beams Under Large Overall Motions—The Plane Case: Part I and II," *Journal of Applied Mechanics*, Vol. 53, No. 4, 1986, pp. 849–863.

[8]Christensen, E., and Lee, S., "Nonlinear Finite Element Modeling of the Dynamic System of Unrestrained Flexible Structures," *Computers and Structures*, Vol. 23, No. 6, 1986, pp. 819–829.

[9]Yoo, H. H., Ryan, R. R., and Scott, R. A., "Dynamics of Flexible Beams Undergoing Overall Motion," *Journal of Sound and Vibration*, Vol. 181, No. 2, 1995, pp. 261–278.

[10]Kane, T. R., and Levinson, D. A., *Dynamics: Theory and Applications*, McGraw–Hill, New York, 1985, Chaps. 2–6.

[11]LS-DYNA 950 Keyword User's Manual, Livermore Software Technology Corp., Livermore, CA, 1999.

[12]LS-DYNA Theoretical Manual, Livermore Software Technology Corp., Livermore, CA, 1998.

S. Saigal
Associate Editor